





This article may be downloaded for personal use only. Any other use requires prior permission of the author and AIP Publishing. This article appeared in Sangdi Gu, Jiaao Hao, Chih-Yung Wen; Can vibrational pumping occur via O₂-N₂ collisions in nonequilibrium vibrationally excited air?. Physics of Fluids 1 June 2023; 35 (6): 066116 and may be found at <https://dx.doi.org/10.1063/5.0151461>.

RESEARCH ARTICLE | JUNE 06 2023

Can vibrational pumping occur via O₂-N₂ collisions in nonequilibrium vibrationally excited air?

Gu Sangdi (顾桑迪)  ; Hao Jiaao (郝佳傲) ; Wen Chih-Yung (温志湧) 



Physics of Fluids 35, 066116 (2023)

<https://doi.org/10.1063/5.0151461>



View Online



Export Citation

CrossMark



APL Quantum
Bridging fundamental quantum research with technological applications

Now Open for Submissions
No Article Processing Charges (APCs) through 2024

Submit Today



Can vibrational pumping occur via O_2 – N_2 collisions in nonequilibrium vibrationally excited air?

Cite as: Phys. Fluids **35**, 066116 (2023); doi: [10.1063/5.0151461](https://doi.org/10.1063/5.0151461)

Submitted: 22 March 2023 · Accepted: 23 May 2023 ·

Published Online: 6 June 2023



View Online



Export Citation



CrossMark

Sangdi Gu (顾桑迪),^{a)} Jiaao Hao (郝佳傲), and Chih-Yung Wen (温志湧)

AFFILIATIONS

Department of Aeronautical and Aviation Engineering, The Hong Kong Polytechnic University, Kowloon, Hong Kong, China

^{a)} Author to whom correspondence should be addressed: sangdi.gu@polyu.edu.hk

ABSTRACT

The occurrence of vibrational pumping in air under nonequilibrium conditions is investigated as this phenomenon is not considered in the design of the current phenomenological models. It is shown that pumping can only happen during de-excitation and when the translational temperature is below around 1000 K. O_2 is the molecule that would get pumped, and pumping will not occur when the initial equilibrium temperature is greater than around 1200–1600 K due to the formation of enough O to extinguish pumping via the O_2 –O vibration–translation reaction. The limiting initial temperature can be increased to around 2000 K if a nonequilibrium initial condition is considered. In cases where pumping does occur, constant–volume reactor simulations showed pumping of $\approx 5\%$. Nozzle simulations representative of that in hypersonic wind tunnels are conducted for an equilibrium temperature of 1100 K at the throat; pumping of up to around 10 K ($\approx 1\%$) can be observed. It can be suggested that constant–volume reactors generally overestimate the manifestation of thermochemical nonequilibrium-associated phenomena and are a better zero-dimensional analogy for the relaxation process in flows with large length scales and no further expansion after an initial rapid expansion. After examination of the uncertainties of the most important rates used in the simulations, one may suggest that the current results correspond to the upper bound for the magnitude of pumping. It may be concluded that pumping is unimportant for practical intents and purposes in nonequilibrium hypersonic flows, and phenomenological models need not be able to recreate this phenomenon.

Published under an exclusive license by AIP Publishing. <https://doi.org/10.1063/5.0151461>

I. INTRODUCTION

Hypersonic flight produces strong shock waves, which almost instantaneously increase the flow's translational (kinetic) and rotational temperature, while the vibrational mode takes longer for excitation.¹ This results in air being in a nonequilibrium state, which will relax toward equilibrium over some time. After that, a nonequilibrium state may be produced again when the equilibrated flow undergoes a rapid expansion (e.g., around a convex corner) where the translational and rotational modes rapidly cool while the vibrational mode requires more time for de-excitation. In the past decades, while nonequilibrium under excitation conditions has been well studied, the reverse scenario of nonequilibrium under de-excitation conditions has not been given the appropriate attention.² The nonequilibrium de-excitation condition is important as it occurs in the expansion region around the shoulder of an atmospheric entry vehicle, which influences the aerothermodynamics to the vehicle afterbody³ as well as the pitching moment of the vehicle.⁴ Nonequilibrium de-excitation also occurs in the flow cycle of hypersonic wind tunnels, making it important for accurately characterizing the test conditions.^{5,6}

At speeds of around 1–2 km/s (temperature around 1000–2000 K), vibrational nonequilibrium is important.^{7–11} Under these conditions during de-excitation, the intermode vibration–vibration–translation (VVT) reaction $O_2(i_1) + N_2(i_2) \leftrightarrow O_2(f_1) + N_2(f_2)$, where i_1 and i_2 are the initial vibrational quantum numbers of molecules 1 and 2, respectively, and f_1 and f_2 are the final vibrational quantum numbers of the respective molecules, may cause a particular phenomenon known as “vibrational pumping” where the vibrational energy of the two molecules, initially in equilibrium, diverges with one increasing and the other decreasing. The occurrence of significant vibrational pumping could influence the aerothermodynamics and pitching moment of atmospheric entry vehicles as well as the test condition in hypersonic wind tunnels, as mentioned above. This could be a significant problem because, as will be shown in Sec. II, pumping is not considered in the formulation of the existing phenomenological models—which are currently important tools used to produce engineering predictions of hypersonic thermochemical nonequilibrium flows (including under de-excitation conditions)—resulting in erroneous estimates of those key parameters if significant pumping happens.

Therefore, it is of substantial interest to investigate whether significant self-pumping can occur in air under nonequilibrium conditions relevant to hypersonic flow.

II. THEORY OF VIBRATIONAL PUMPING

To demonstrate the concept of vibrational pumping, let us first consider the generic $AB(i_1) + AB(i_2) \leftrightarrow AB(f_1) + AB(f_2)$ intramode VVT reaction, where AB is some molecule. The net reaction rate can be written as

$$\frac{d[AB(i_1)]}{dt} = k_f[AB(f_1)][AB(f_2)] - k_r[AB(i_1)][AB(i_2)], \quad (1)$$

where the square brackets denote the molar concentration of the species, and k_f and k_r are the forward and reverse rate coefficients, respectively. Applying detailed balancing via the use of the partition functions¹² and rearranging

$$\frac{d[AB(i_1)]}{dt} = \left(e^{\frac{\Delta E}{K_B T}} \frac{[AB(f_1)][AB(f_2)]}{[AB(i_1)][AB(i_2)]} - 1 \right) k_f[AB(i_1)][AB(i_2)], \quad (2)$$

where T is the translational temperature, K_B is the Boltzmann constant, and ΔE is the energy defect of the reaction [$\Delta E = E_{AB(f_1)} + E_{AB(f_2)} - E_{AB(i_1)} - E_{AB(i_2)}$, where E is the energy of a vibrational level]. Defining a vibrational temperature, $T_v^{i_1, i_2, f_1, f_2}$, which gives the same ratio of the population among the four states if the states were populated by a Boltzmann distribution¹³

$$\frac{[AB(f_1)][AB(f_2)]}{[AB(i_1)][AB(i_2)]} = e^{\frac{-\Delta E}{K_B T_v^{i_1, i_2, f_1, f_2}}} \quad (3)$$

and substituting into Eq. (2)

$$\frac{d[AB(i_1)]}{dt} = \left(e^{\frac{\Delta E}{K_B} \left(\frac{1}{T} - \frac{1}{T_v^{i_1, i_2, f_1, f_2}} \right)} - 1 \right) k_f[AB(i_1)][AB(i_2)]. \quad (4)$$

In Eq. (4), k_f , $[AB(i_1)]$, and $[AB(i_2)]$ are always positive values; $\frac{d[AB(i_1)]}{dt}$ is positive when the net rate is in the reverse direction; and ΔE is positive when the forward reaction increases the total vibrational energy of AB. From inspection of Eq. (4), the reaction proceeds in the forward direction when $\frac{\Delta E}{K_B} \left(\frac{1}{T} - \frac{1}{T_v^{i_1, i_2, f_1, f_2}} \right) < 0$ and vice versa for the reverse direction. If $\Delta E > 0$ and $T_v^{i_1, i_2, f_1, f_2} > T$, then $\frac{\Delta E}{K_B} \left(\frac{1}{T} - \frac{1}{T_v^{i_1, i_2, f_1, f_2}} \right) > 0$, which means that the reaction proceeds in the reverse direction and vibrational energy is removed—vibrational energy will only be gained when $T_v^{i_1, i_2, f_1, f_2} < T$. The same is obtained when considering $\Delta E < 0$. Therefore, although intramode vibration–vibration (VV) exchange and anharmonicity are known to cause overpopulation of the intermediate and upper levels,¹⁴ intramode VVT reactions, just like vibrational–translation (VT) reactions, will always proceed such that the aggregate change in vibrational energy is in the direction of equilibrium.

Now consider the generic $AB(i_1) + CD(i_2) \leftrightarrow AB(f_1) + CD(f_2)$ intermode VVT reaction, where AB and CD are different molecules. Applying the same derivation above

$$\frac{d[AB(i_1)]}{dt} = \left(e^{\frac{\Delta E}{K_B} \left(\frac{1}{T} - \frac{1}{T_v^{i_1, i_2, f_1, f_2}} \right)} - 1 \right) k_f[AB(i_1)][CD(i_2)], \quad (5)$$

where

$$\frac{[AB(f_1)][CD(f_2)]}{[AB(i_1)][CD(i_2)]} = e^{\frac{-\Delta E}{K_B T_v^{i_1, i_2, f_1, f_2}}} \quad (6)$$

and $\Delta E = \Delta E_{AB} + \Delta E_{CD}$ with $\Delta E_{AB} = E_{AB(f_1)} - E_{AB(i_1)}$ and $\Delta E_{CD} = E_{CD(f_2)} - E_{CD(i_2)}$. Inspecting Eq. (5), one can see that intermode VVT reactions can also only proceed in the direction of overall equilibrium. However, if ΔE_{AB} and ΔE_{CD} are of different signs and both molecules have either too much or too little vibrational energy (compared with the translational mode), then the vibrational energy of one of the molecules will be “pumped” further away from equilibrium, while the reaction will still proceed in such a way that the total vibrational energy moves toward equilibrium. For example, if $\Delta E < 0$, $\Delta E_{AB} > 0$ (which means $\Delta E_{CD} < 0$ and $|\Delta E_{CD}| > |\Delta E_{AB}|$), and $T_v^{i_1, i_2, f_1, f_2} > T$, then the right-hand side of Eq. (5) is negative and the reaction proceeds in the forward direction, reducing the total vibrational energy at the expense of “pumping” the vibrational energy of AB. This process is illustrated in Fig. 1 by the solid arrows. If the vibrational energy of AB is already in excess—likely given $T_v^{i_1, i_2, f_1, f_2} > T$ —then this mechanism will cause it to further diverge from equilibrium. In this way, the molecule with the smaller energy spacings gets pumped.¹²

The occurrence of the pumping discussed above is of concern as current multi-temperature (reduced-order, phenomenological) models for nonequilibrium hypersonic flows, which are often used for engineering purposes, are not formulated to predict this phenomenon and, consequently, cannot even qualitatively capture the behavior. The most commonly used multi-temperature model is the two-temperature model in which the vibrational modes are assumed to be tightly coupled among the molecules where they are described by a single vibrational temperature;¹⁵ this assumption may be valid in post-shock (excitation) conditions.⁴ However, it is well recognized that, under expanding flow (de-excitation) conditions, molecular vibrational modes are in nonequilibrium with each other and have different vibrational temperatures even without the occurrence of vibrational pumping.^{5,15} This led to the use of multi-vibrational temperature models for expanding flows.^{2,16,17} In these models, the VV energy exchange between molecules AB and CD is governed by a simple equation of the form¹⁸

$$\left\{ \frac{de_{v,AB}}{dt} \right\}_{VV} = \alpha \left(e_{v,AB}^{eq} - e_{v,AB} \right), \quad (7)$$

where α is a positive coefficient that depends on the collision probability and collision number, $e_{v,AB}$ is the vibrational energy of AB, and $e_{v,AB}^{eq}$ is the vibrational energy of AB assuming the vibrational modes of AB and CD are in equilibrium and the total vibrational energy

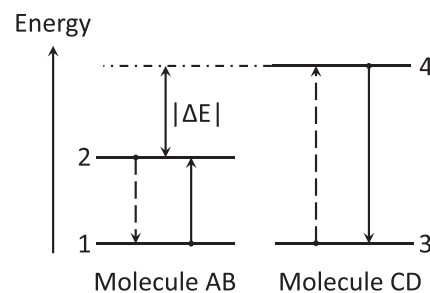


FIG. 1. Exchange pumping in a four-state system. Adapted from Ref. 12.

among AB and CD is conserved. However, in this equation, energy always transfers in a way that brings the vibrational modes closer together. This is only true for ideal VV exchanges, where $\Delta E = 0$;¹⁹ in reality, $\Delta E \neq 0$ resulting in pumping. Equation (7) would, consequently, be inapplicable under conditions where pumping is dominant.

Vibrational pumping is well recognized by the gasdynamic laser (GDL) community, which has successfully used it to engineer extremely nonequilibrium conditions necessary for the operation of their lasers.^{20–25} GDLs mostly operate with CO–N₂–Ar or CO₂–N₂–He mixtures in which population inversion is created between two specific vibrational states in CO or CO₂, which function as the lasing medium.^{20,23} This population inversion is generated via vibrational pumping by an expansion of the aforementioned mixtures in a nozzle from some reservoir condition. Significant fundamental work has been done to fully understand the mechanisms involved in this process.²³ This provided the foundations to allow work done on tuning the temperature, pressure, and species mole fractions of the reservoir, and the contour of the nozzle to maximize the optical gain of the lasing medium.^{26–28} The tuning was mainly done via numerical means, with the state-to-state (StS) approach being used to successfully model the thermochemical kinetics.^{12,20,22,24,29} Laser beams with hundreds of kilowatts of power, operating for milliseconds, have been produced.²¹

III. METHODOLOGY

There are a few important differences in the style of the current work, for applications in hypersonic flow to address the motivation specified in Sec. I, compared with the style of the past work done on vibrational pumping for GDL applications. First, the current work focuses on the air mixture rather than the CO–N₂–Ar or CO₂–N₂–He mixtures, which have very different thermochemical kinetics. Second, the current work is interested in the natural occurrence of pumping rather than the engineering of this phenomenon to optimize optical gain. Third, because it is shown that the total vibrational energy is a much more important parameter than the vibrational population distribution in hypersonic flows,¹⁵ the vibrational pumping concerned in this paper is the pumping of the total vibrational energy of a molecular rather than the pumping of a particular vibrational level of a molecule, which is more important for GDL applications.

In this paper, the competing processes are examined to assess the possibility of vibrational pumping occurring naturally in nonequilibrium air for a general range of conditions. Then, constant–volume reactor simulations are conducted at an equilibrium and a nonequilibrium initial condition for a detailed examination of the vibrational relaxation process and to quantify the extent of pumping. Finally, simulations of nozzle expansions are conducted to discuss the possibility of vibrational pumping in nozzle flows (which are important in hypersonic wind tunnels) as well as explain the interpretation of the zero-dimensional constant–volume reactor results for real gasdynamic environments.

The governing equations for a constant–volume reactor are

$$\begin{aligned} \frac{d\rho}{dt} &= 0, \\ \frac{dh_0}{dt} &= 0, \\ \frac{dc_i}{dt} &= \frac{\dot{w}_i}{\rho}, \end{aligned} \tag{8}$$

while the ones for a quasi-one-dimensional steady nozzle are^{15,30}

$$\begin{aligned} \frac{d\rho u A}{dx} &= 0, \\ \frac{dp}{dx} + \rho u \frac{du}{dx} &= 0, \\ \frac{dh_0}{dx} &= 0, \\ \frac{dc_i}{dx} &= \frac{\dot{w}_i}{\rho u}, \end{aligned} \tag{9}$$

where t is the time, ρ is the mass density, u is the flow velocity, A is the nozzle cross-sectional area, p is the pressure, h_0 is the total specific enthalpy, c is the mass fraction, \dot{w} is the mass production rate, and the subscript i is the species index. These are systems of ordinary differential equations (ODE), where the rate equations are coupled to the hydrodynamic equations through the equation of state ($p = \rho RT$, where R is the specific gas constant of the gas mixture and T is the translational temperature) and the total enthalpy equation ($h_0 = e + RT + u^2/2$, where e is the specific internal energy of the gas mixture that includes the translational, rotational, and vibrational energies as well as the heat of formation³¹). These ODE systems, which are stiff, are integrated using the Crank–Nicolson method with the step size controlled by the criterion given in Refs. 32 and 33 to maintain numerical stability. With numerical stability maintained, the solution of these stiff ODE systems is generally accurate and reliable as any deviation from the correct solution will immediately drive the numerical solution back toward the correct solution.³⁴ In the following constant–volume reactor and nozzle simulations presented in this paper, around 1000–2000 steps were used to obtain the solution.

An StS model, described in detail in Refs. 15 and 35, is used in the current work. Five species—N₂, O₂, N, O, and NO—are considered. The energies of the vibrational levels for N₂ and O₂ used in this work are obtained from the STELLAR database,³⁶ and they are determined by solving the radial Schrödinger equation with potential curves obtained from the Rydberg–Klyning–Rees method.³⁷ There are 61 bound vibrational levels for N₂, 46 for O₂, and 48 for NO. Only the ground electronic state is considered. Along with the VVT and VT reactions, the N₂, O₂, and NO dissociation/recombination reactions and the two Zel’dovich reactions are modeled. The reactions modeled are summarized in Tables I and II. The state-specific rates used originate from a combination of forced harmonic oscillator (FHO) theory,³⁸ quasi-classical trajectory (QCT) calculations,³⁹ and the classic Landau–Teller (LT) model in StS form.⁴⁰ The accuracy of these rates is examined in Refs. 15 and 35. The forward and backward rates are related by detailed balance using the partition functions. Equilibration between translational and rotational modes is assumed.

Consider a molecular species $AB \in \{N_2, O_2\}$ at a vibrational level i_1 , the resulting species production rate can be written generally as^{5,45–47}

$$\begin{aligned} \dot{w}_{AB(i_1)} &= \mathcal{M}_{AB} \left[\left\{ \dot{w}_{AB(i_1)} \right\}_{VVT} + \left\{ \dot{w}_{AB(i_1)} \right\}_{VT} \right. \\ &\quad \left. + \left\{ \dot{w}_{AB(i_1)} \right\}_{VD} + \left\{ \dot{w}_{AB(i_1)} \right\}_{EX} \right], \end{aligned} \tag{10}$$

where

TABLE I. The inelastic reactions considered in this work, where $M \in \{NO, O, N\}$.

No.	Reaction	Model	Ref.
1	$N_2(i_1) + N_2(i_2) \leftrightarrow N_2(f_1) + N_2(f_2)$	FHO	35
2	$O_2(i_1) + O_2(i_2) \leftrightarrow O_2(f_1) + O_2(f_2)$	FHO	35
3	$O_2(i_1) + N_2(i_2) \leftrightarrow O_2(f_1) + N_2(f_2)$	FHO	35
4	$NO(i) + N_2 \leftrightarrow NO(f) + N_2$	FHO	41
5	$NO(i) + O_2 \leftrightarrow NO(f) + O_2$	FHO	41
6	$NO(i) + M \leftrightarrow NO(f) + M$	LT	13, 40
7	$N_2(i) + N \leftrightarrow N_2(f) + N$	QCT	42
8	$O_2(i) + O \leftrightarrow O_2(f) + O$	QCT	39
9	$N_2(i) + O \leftrightarrow N_2(f) + O$	LT	13, 40
10	$O_2(i) + N \leftrightarrow O_2(f) + N$	LT	13, 40
11	$N_2(i) + NO \leftrightarrow N_2(f) + NO$	LT	13, 40
12	$O_2(i) + NO \leftrightarrow O_2(f) + NO$	LT	13, 40

$$\{w_{AB(i_1)}\}_{VVT} = \sum_{i_2=0}^{i_2,max} \sum_{\substack{f_1=0 \\ f_1 \neq i_1}}^{f_1,max} \sum_{f_2=0}^{f_2,max} k_{VVT}(f_1, f_2 \rightarrow i_1, i_2) X_{f_1} X_{f_2} - k_{VVT}(i_1, i_2 \rightarrow f_1, f_2) X_{i_1} X_{i_2} \quad (11)$$

for the molecule–molecule interactions

$$\{w_{AB(i_1)}\}_{VT} = \sum_M \sum_{\substack{f_1=0 \\ f_1 \neq i_1}}^{f_1,max} k_{VT}(f_1, M \rightarrow i_1, M) X_{f_1} X_M - k_{VT}(i_1, M \rightarrow f_1, M) X_{i_1} X_M \quad (12)$$

for the molecule–atom interactions and the molecule–molecule interactions where VVT reactions are not considered

TABLE II. The dissociation/recombination and exchange reactions considered in this work, where $M \in \{NO, O, N\}$.

No.	Reaction	Model	Ref.
1	$N_2(i) + N_2 \leftrightarrow 2N + N_2$	FHO	41
2	$O_2(i) + O_2 \leftrightarrow 2O + O_2$	FHO	41
3	$N_2(i) + O_2 \leftrightarrow 2N + O_2$	FHO	41
4	$O_2(i) + N_2 \leftrightarrow 2O + N_2$	FHO	41
5	$N_2(i) + N \leftrightarrow 3N$	QCT	42
6	$O_2(i) + O \leftrightarrow 3O$	QCT	39
7	$N_2(i) + O \leftrightarrow 2N + O$	Reaction 5	13
8	$O_2(i) + N \leftrightarrow 2O + N$	Reaction 6	13
9	$N_2(i) + NO \leftrightarrow 2N + NO$	Reaction 1	13
10	$O_2(i) + NO \leftrightarrow 2O + NO$	Reaction 4	13
11	$NO(i) + N_2 \leftrightarrow N + O + N_2$	FHO	41
12	$NO(i) + O_2 \leftrightarrow N + O + O_2$	FHO	41
13	$NO(i) + M \leftrightarrow N + O + M$	(Reaction 11) \times 20	13
14	$N_2(i) + O \leftrightarrow NO(f) + N$	QCT	43
15	$O_2(i) + N \leftrightarrow NO(f) + O$	QCT	44

$$\{w_{AB(i_1)}\}_{VD} = \sum_M k_{VD}(A, B, M \rightarrow i_1, M) X_A X_B X_M - k_{VD}(i_1, M \rightarrow A, B, M) X_{i_1} X_M \quad (13)$$

for the dissociation/recombination reactions, and

$$\{w_{AB(i_1)}\}_{EX} = \sum_{f=0}^{f,max} k_{EX}(NO(f), N/O \rightarrow i_1, O/N) X_{NO(f)} X_{N/O} - k_{EX}(i_1, O/N \rightarrow NO(f), N/O) X_{i_1} X_{O/N} \quad (14)$$

for the NO exchange reactions. Here, A and B represent atomic species, M is the molar mass, k is the reaction rate coefficient (calculated from the FHO, QCT, or LT model depending on the reaction, as stated in Tables I and II), and X is the molar concentration. From these, one can easily derive the species production rate for N, O, and NO(i_1).

Containing 155 pseudo-species and more than 10^7 reactions, the current StS model is computationally too expensive for implementation in multi-dimensional Navier–Stokes simulations and is, therefore, only used in constant-volume reactor and quasi-one-dimensional nozzle simulations in the present work. Nevertheless, such simulations are adequate for revealing important features of thermochemical non-equilibrium as demonstrated exemplarily in Refs. 5, 48, and 49.

IV. RESULTS

In Secs. IV A–IV D, the competing reactions for pumping in non-equilibrium air are first examined. Afterward, constant-volume reactor simulations are conducted at, first, an equilibrium and, then, a nonequilibrium initial condition. Finally, simulations of nozzle expansions are presented.

A. Competing processes

All transitions of $O_2(i_1) + N_2(i_2) \leftrightarrow O_2(f_1) + N_2(f_2)$ can be categorized into two sets, A and B, where set A contains combinations of $i_1, i_2, f_1,$ and $f_2,$ giving transitions satisfying $(\Delta E_{O_2} \Delta E_{N_2}) \geq 0$ and set B contains the combinations satisfying $(\Delta E_{O_2} \Delta E_{N_2}) < 0$. In other words, set A contains the transitions where the vibrational energy of O_2 and N_2 change in the same direction (both increase or decrease) or one has no change, while set B contains the transitions where they change in opposite directions. Transitions in set A are essentially like VT reactions where no energy is exchanged among the vibrational modes, while transitions in set B all contain vibration–vibration (VV) energy exchange. Set A, along with the intramode VVT reactions, drives the vibrational mode toward equilibration with the translational mode. On the other hand, set B tends to pump the vibrational mode of one of the molecules away from equilibrium. Although set B contains transitions that pump O_2 as well as transitions that pump N_2 , the molecule that gets pumped overall would be O_2 due to its shallower vibrational well and smaller spacing between the vibrational levels.

The occurrence of vibrational pumping is subjected to competition among the rates and is, thus, condition-dependent. It is generally known that vibrational pumping is most severe under conditions of high vibrational temperature and low translational temperature.¹⁴ To demonstrate this for the O_2 – N_2 VVT reaction, Fig. 2 is plotted showing the ratio of the O_2 vibrational energy source terms between sets B and A, calculated as

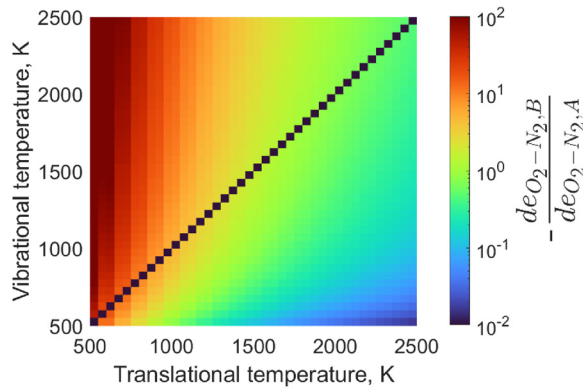
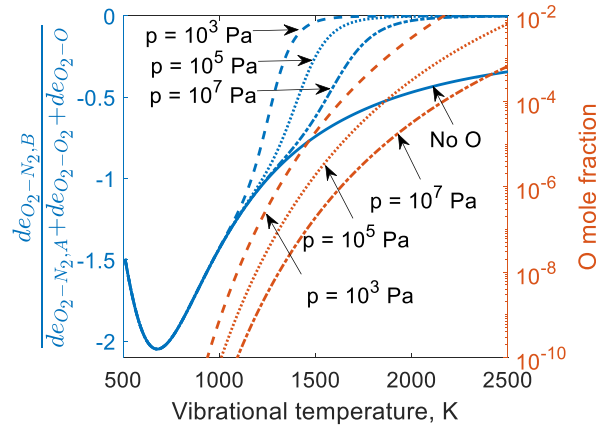


FIG. 2. The ratio of the O₂ vibrational energy source terms between sets A and B of the O₂-N₂ VVT reaction at different vibrational and translational temperatures. The vibrational population is assumed to be Boltzmann distributed at the given vibrational temperature.

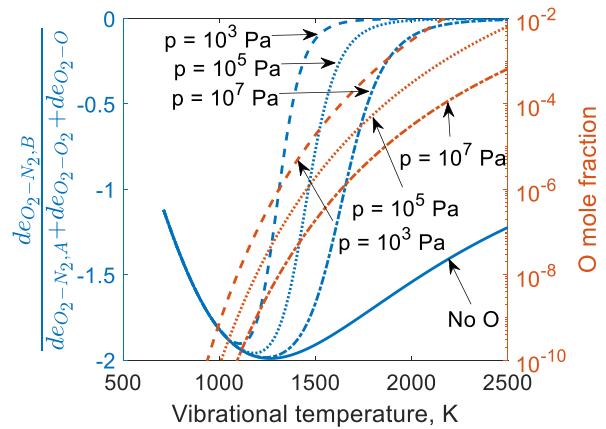
$$\frac{de_{O_2-N_2,B}}{de_{O_2-N_2,A}} = \frac{\sum_{i=0}^{i,max} E_{O_2(i)} \{w_{O_2(i)}\}_{O_2-N_2 VVT,B}}{\sum_{i=0}^{i,max} E_{O_2(i)} \{w_{O_2(i)}\}_{O_2-N_2 VVT,A}} \quad (15)$$

at different vibrational and translational temperatures. From the figure, one can see that set B dominates, by more than two orders of magnitude, over set A when the translational temperature is low and the vibrational temperature is high. The converse is observed at high translational temperature and low vibrational temperature, where set A dominates over set B by more than two orders of magnitude. The figure also shows that the ratio is a negative value throughout, confirming that O₂ is the molecule being pumped away from equilibrium by set B, and set A and set B are competing processes in the O₂ vibrational energy transfer. The ratio is independent of pressure because both set A and set B are second-order reactions and the numerator and denominator in Eq. (15) both scale equally with pressure.

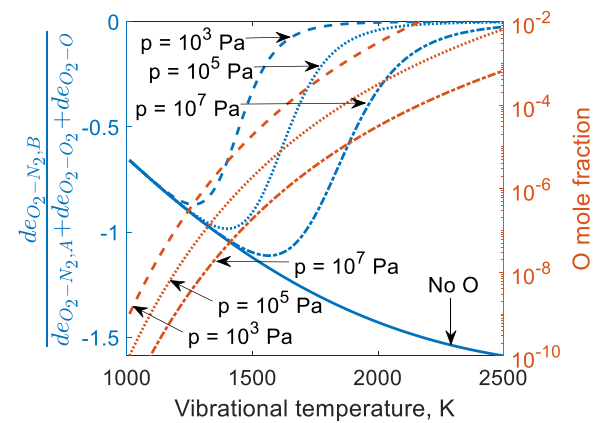
Based on the above result, it may seem that the vibrational pumping of O₂ is most likely to occur when the vibrational temperature is high and the translational temperature is low. However, set B not only competes with set A but also competes with the O₂-O₂ intramode VVT reaction as well as the O₂-O VT reaction. The inclusion of the O₂-O VT reaction as being a competitor may seem somewhat surprising given dissociation is often considered negligible at the current temperature range of interest and O would be in very small amounts.³¹ However, it is shown, theoretically^{50,51} and experimentally,⁵²⁻⁵⁴ that the O₂-O VT reaction is extremely efficient at low translational temperatures, and trace amounts of O can influence the vibrational relaxation process significantly. This is further demonstrated in Fig. 3, which shows, at three different translational temperatures, the ratio of the O₂ vibrational energy source terms between set B (the pumping process) and the three equilibrating processes—O₂-N₂ VVT set A, O₂-O₂ VVT, and O₂-O VT—for an equilibrium five-species air composition, calculated using Cantera,⁵⁵ equilibrated at the given vibrational temperature and defined pressure. Here, the numerator and denominator are also all second-order reactions which means they scale equally with pressure, and, hence, the pressure dependency shown in the



(a)



(b)



(c)

FIG. 3. The ratio of the O₂ vibrational energy source terms between set B and the three equilibrating processes at translational temperatures of (a) 500 K, (b) 700 K, and (c) 1000 K for an equilibrium five-species air composition equilibrated at the given vibrational temperature and defined pressure. The vibrational population is assumed to be Boltzmann distributed at the given vibrational temperature.

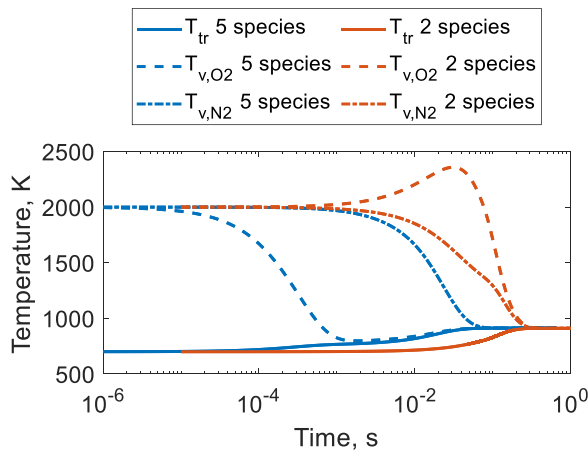


FIG. 4. Relaxation in a constant-volume reactor with the translational and vibrational temperatures initially at 700 and 2000 K, respectively, and the pressure initially at 14 kPa. The chemical composition of the five-species simulation is initially in equilibrium with the initial pressure and vibrational temperature.

figure comes entirely from the pressure dependency of the O mole fraction. One can see that, at all three translational temperatures, an O mole fraction of just 10^{-7} , occurring at a temperature of around 1200–1400 K depending on the pressure, is enough to start influencing the ratio of the O_2 vibrational energy source terms due to the contribution from the O_2 -O VT reaction, which is calculated in this work using the accurate QCT rates computed by Ref. 39, which compares well with the other sources reported in the literature as shown in Ref. 50. Beyond this temperature and corresponding O mole fraction, the ratio rapidly goes toward zero as the O_2 -O VT reaction completely dominates the O_2 vibrational energy transfer. As the O mole fraction gets to around 10^{-4} , occurring at a temperature of around 1500–2000 K depending on the pressure, the ratio is essentially zero, which indicates negligible contribution from set B.

The influence of small quantities of O is further demonstrated in Fig. 4, which shows the vibrational relaxation in a zero-dimensional constant-volume reactor, obtained by solving the ODE system given by Eq. (8) via marching to $t = 1$ s, using the five-species air model described in Sec. III and a two-species air model, which consists of only O_2 and N_2 at a fixed mole fraction ($N_2:0.78$ and $O_2:0.22$) reacting via the O_2 - O_2 , N_2 - N_2 , and O_2 - N_2 VVT reactions. This simulation physically corresponds to the time evolution of the gas in a stationary adiabatic container of fixed volume, assuming the gas in the container is spatially uniform throughout. The translational and vibrational temperatures are initially at 700 and 2000 K, respectively; the pressure is initially at 14 kPa, and the chemical composition of the five-species simulation is initially in equilibrium with the initial pressure and vibrational temperature. The vibrational temperature shown in Fig. 4 is the average vibrational temperature, obtained by solving the following equation for $T_{V,AB}$ ^{15,35,56}

$$\sum_{v=0}^{v_{\max}(AB)} \frac{\rho_{ABv}}{\rho_{AB}} E_{ABv} = \frac{\sum_{v=0}^{v_{\max}(AB)} E_{ABv} \exp\left(-\frac{E_{ABv}}{k_B T_{v,AB}}\right)}{\sum_{v=0}^{v_{\max}(AB)} \exp\left(-\frac{E_{ABv}}{k_B T_{v,AB}}\right)}, \quad (16)$$

where the energy of the nonequilibrium vibrational distribution equals the energy of a Boltzmann equilibrium vibrational distribution at the vibrational temperature $T_{V,AB}$. Figure 4 shows that the inclusion of O dramatically increases the O_2 vibrational relaxation rate. This is due to the O_2 -O VT reaction as shown in Fig. 5(a), which completely overwhelms the other reactions. The O mole fraction is essentially frozen throughout the vibrational relaxation of O_2 , and recombination only begins after the vibrational mode of O_2 achieves equilibrium with the translational mode as shown in Fig. 6. The vibrational relaxation of N_2 is, to a lesser extent, also made faster by the presence of O due to the N_2 -O VT reaction, which is also quite efficient at low translational temperatures as shown in Ref. 50. If no O exists, substantial vibrational pumping of O_2 can occur at this condition as shown in Fig. 4, where

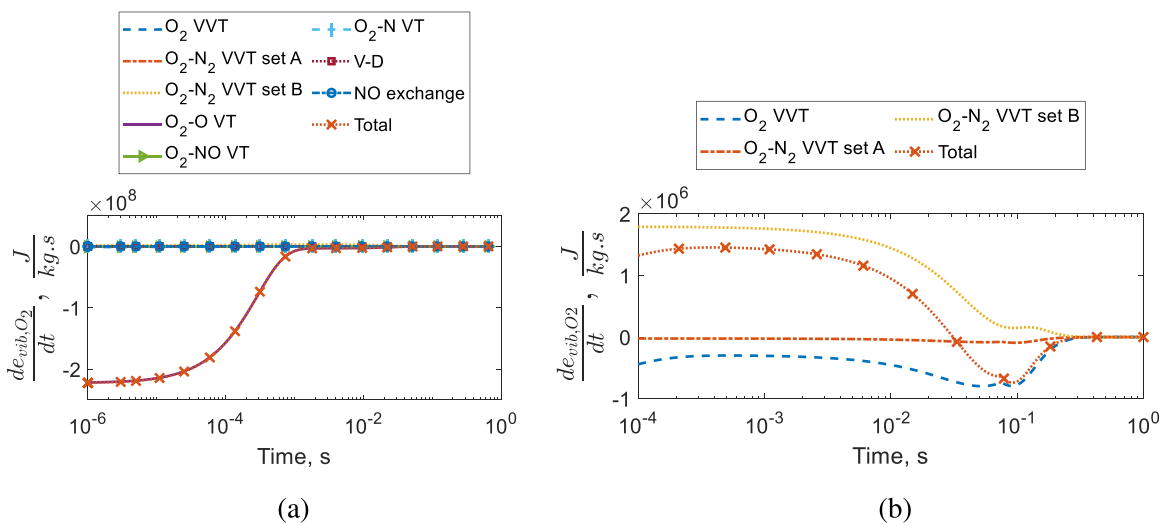


FIG. 5. The O_2 vibrational energy source terms from different reactions in the (a) five-species and (b) two-species simulations.

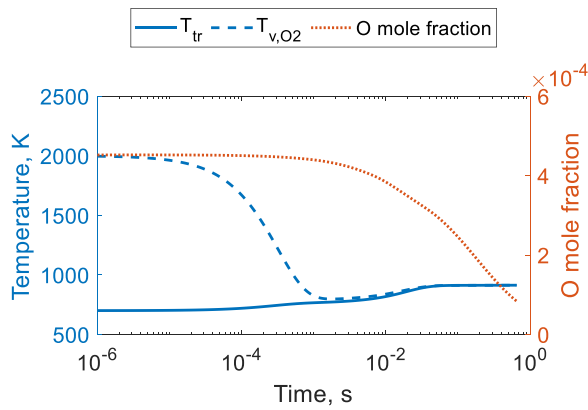


FIG. 6. The translational and O₂ vibrational temperatures along with the O mole fraction from the five-species simulation of the constant-volume reactor in Fig. 4.

the vibrational temperature of O₂ increases to almost 2500 from 2000 K, as the O₂-N₂ VVT set B reaction initially dominates the vibrational energy transfer with its main competitor being the O₂-O₂ VVT reaction as shown in Fig. 5(b).

The influence of the O₂-O VT reaction is further evident when examining the vibrational population distribution of O₂. As shown in Fig. 7, without the O₂-O VT reaction, the distribution is a Treanor distribution where the lower level population is approximately Boltzmann distributed at around the average vibrational temperature, while the intermediate and upper levels have a population inversion. Such a quasi-steady distribution forms due to the VV energy exchanges (both intramode and intermode) and anharmonicity in the vibrational energy levels as examined in detail in Refs. 14, 23, and 57. With the presence of the O₂-O VT reaction, the population inversion in the upper levels disappears and a Boltzmann distribution at around the translational temperature is formed in its place as the upper vibrational levels are known to be in close communication with the translational mode due to the fast VT rates there because of the small spacing between the levels.^{23,58} Subsequently, the resulting distribution function is in the shape of χ

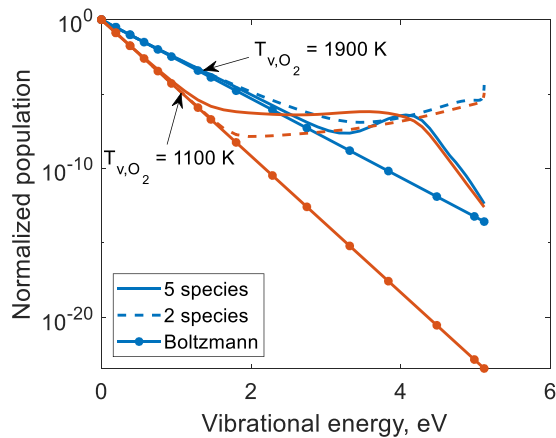


FIG. 7. The normalized O₂ vibrational population distribution in the simulation of the constant-volume reactor in Fig. 4 when $T_{v,O_2} = 1100$ K and $T_{v,O_2} = 1900$ K.

which, like the Treanor distribution, is a well-understood distribution examined in detail in Refs. 29 and 59, and it is formed early and maintained as quasi-steady during the relaxation process.

B. Equilibrium initial condition (constant-volume reactor)

Overall, Fig. 3 indicates that there is only a small and limited region of conditions that can produce O₂ pumping to any degree. For the case of the translational temperature being 500 and 700 K, vibrational pumping can occur when the vibrational temperature is higher than the translational temperature but below around 1200–1600 K (depending on the pressure). However, for the case of the translational temperature being 1000 K, vibrational pumping will basically not occur at all because the equilibrating contributions from the O₂-O₂ VVT and O₂-N₂ VVT set A reactions quench the pumping contribution from the O₂-N₂ VVT set B reaction enough before even the onset of the O₂-O VT reaction as indicated by the ratio of the source terms in Fig. 3(c).

Therefore, a zero-dimensional constant-volume reactor simulation is conducted, by solving the ODE system given by Eq. (8), at a condition where vibrational pumping is expected—an initial translational temperature of 700 K and an initial vibrational temperature of 1100 K with the chemical composition initially equilibrated with the vibrational temperature and a pressure of 40 kPa. Marching to $t = 1$ s from the aforementioned initial condition, the time evolution of the gas in the container is shown in Fig. 8(a), assuming the fixed volume of gas is spatially uniform throughout. One can see that vibrational pumping is observed where the O₂ vibrational temperature initially increases by up to around 50 K ($\approx 5\%$). The amount of O is so small (mole fraction $\approx 10^{-9}$) that there is no difference between the five-species and two-species results. Looking at the O₂ vibrational energy source terms shown in Fig. 8(b), the main participants are the O₂-O₂ VVT and O₂-N₂ VVT set B reactions. The O₂-N₂ VVT set B reaction initially wins over the O₂-O₂ VVT reaction resulting in pumping. As discussed in Ref. 29, energy flows up the vibrational ladder from the lower levels during pumping. This is evident in Fig. 9, which shows the normalized population of O₂ when looking at how the distribution changes between $t = 0$ to $t = 30$ ms. As the intermediate and upper levels get populated, the pumping contribution weakens while the equilibrating O₂-O₂ VVT reaction strengthens as shown in Fig. 8(a). A peak in vibrational temperature is then reached, at around 20–30 ms, after which the vibrational temperature decreases toward equilibrium. The relaxation toward equilibrium occurs essentially via quasi-steady Treanor distributions, as shown in Fig. 9, indicating the prominence of the VV energy exchanges as discussed in Ref. 57.

As Fig. 8(b) shows that the main participants are the O₂-O₂ VVT and O₂-N₂ VVT set B reactions, it is of interest to examine which particular transitions in these sets of reactions are the most important contributors to the transfer of energy in and out of the O₂ vibrational mode. Hence, Fig. 10 is created showing the contribution of each transition at different times during the relaxation. The O₂(1) + N₂(0) \leftrightarrow O₂(0) + N₂(1) transition is found to be the most dominant O₂-N₂ VVT set B transition, accounting for more than 70% of the total contribution from O₂-N₂ set B. The O₂(1) + O₂(0) \leftrightarrow O₂(0) + O₂(0) transition is found to be the main O₂-O₂ VVT transition responsible for energy transfer, accounting for more than 60% of the

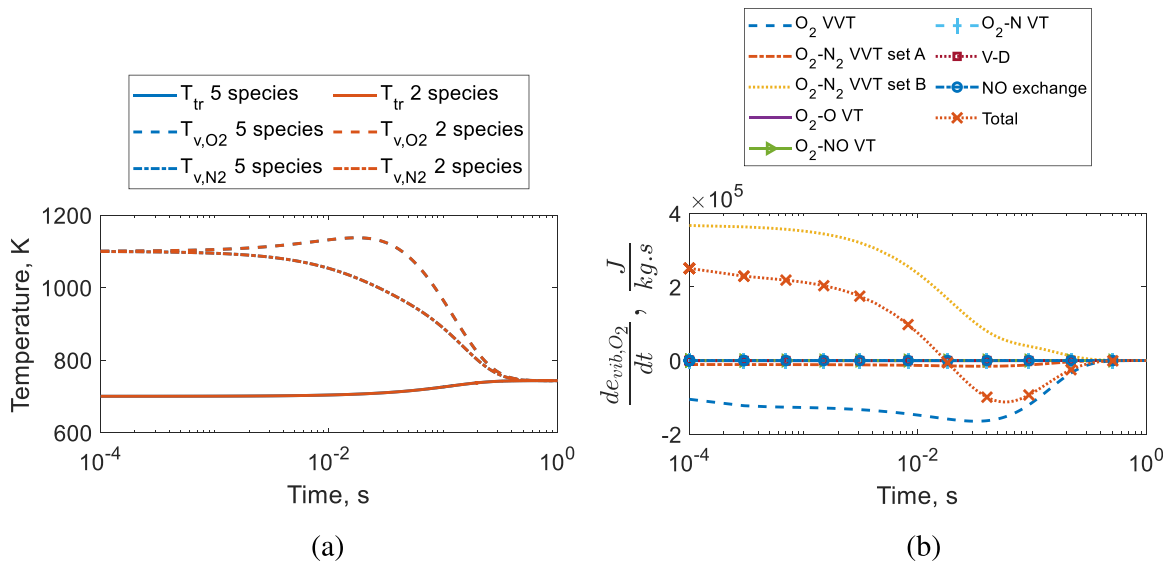


FIG. 8. Relaxation in a $\rho = 0.13 \text{ kg/m}^3$ constant-volume reactor with the translational and vibrational temperatures initially at 700 and 1100 K, respectively. The temperatures and O₂ vibrational energy contributions are shown in (a) and (b), respectively.

total contribution from O₂-O₂ VVT. The dominance of these two reactions is maintained throughout the relaxation.

As mentioned earlier and shown in Fig. 8(a), pumping increases the vibrational temperature of O₂ by up to around 50 K in the current simulation. Based on the result in Fig. 10, the magnitude of this increase depends strongly on the accuracy of the rates of O₂(1) + N₂(0) ↔ O₂(0) + N₂(1) and O₂(1) + O₂(0) ↔ O₂(0) + O₂(0) used in the simulation. Therefore, comparisons of the FHO rates used in the current simulation with QCT and semi-classical (SC) theoretical results as well as experimental measurements are presented in Fig. 11. For the O₂(1) + O₂(0) ↔ O₂(0) + O₂(0) transition, the FHO rate agrees well with the SC and experimental results from low to high temperatures. On the other hand, for the O₂(1) + N₂(0) ↔ O₂(0) + N₂(1) transition, large discrepancies exist between the experimental

measurements and the theoretical (QCT and SC) calculations at lower temperatures, with the FHO results agreeing very closely with the experimental measurements. At translational temperatures below 1000 K, which is the case for the conditions simulated in this paper, the FHO and experimental rates differ from the QCT and SC rates by more than five orders of magnitude. Interpreting the FHO rate as being the upper bound of the uncertainty of the actual O₂(1) + N₂(0) ↔ O₂(0) + N₂(1) rate, one may suggest that the current simulation already gives the upper bound for the magnitude of vibrational pumping which, being less than 50 K (≈5%), is quite small.

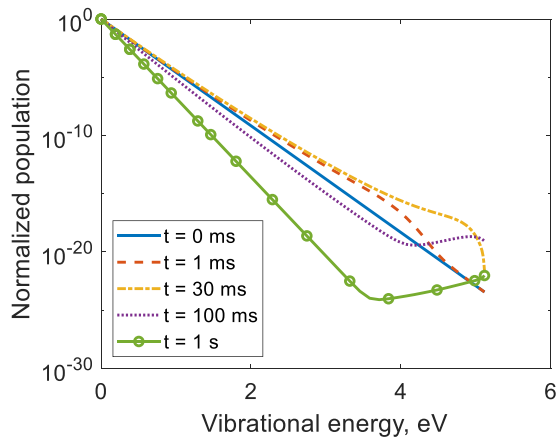


FIG. 9. Normalized O₂ vibrational population at various times in the simulation in Fig. 8.

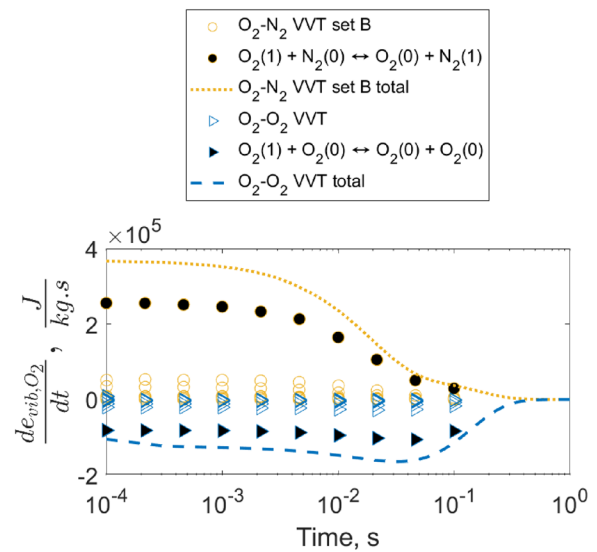


FIG. 10. The O₂ vibrational energy contributions showing the contribution of each transition in the O₂-N₂ B and O₂-O₂ VVT reaction sets.

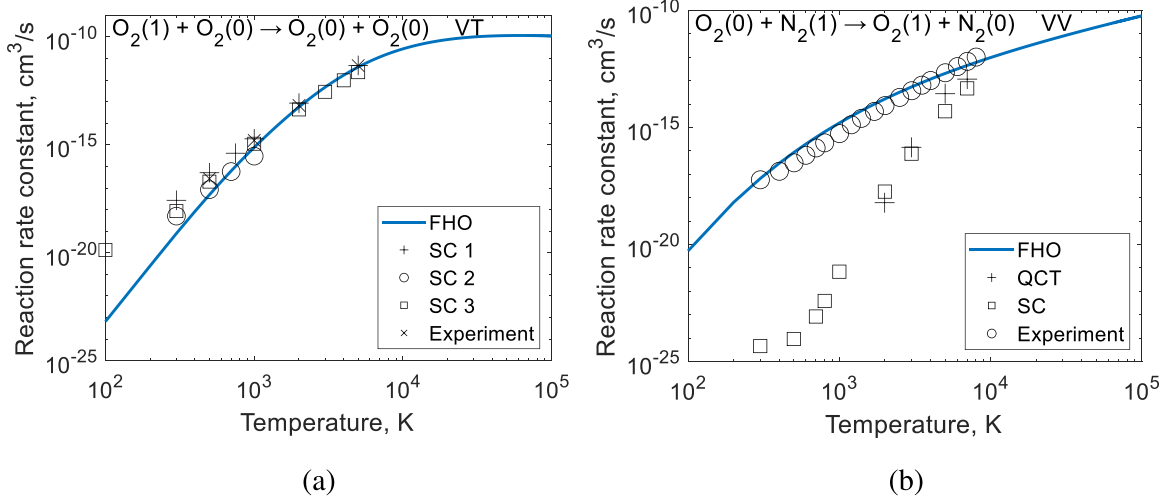


FIG. 11. Reaction rate coefficients of (a) $O_2(1) + O_2(0) \leftrightarrow O_2(0) + O_2(0)$ and (b) $O_2(0) + N_2(1) \leftrightarrow O_2(1) + N_2(0)$. In (a), “SC 1,” “SC 2” and “SC 3” are from Refs. 60,61, and 62, respectively, while “Experiment” is from Ref. 63. In (b), “QCT” is from Ref. 64, “SC” is from Ref. 65, and experiment is from Ref. 66.

The reason behind the discrepancies seen in Fig. 11(b) remains unclear. The discrepancy between the SC result and the experimental result, which was obtained in the 1960s, is particularly interesting. Because the SC method is currently the highest fidelity way of theoretically calculating these rates, it has been suggested that significant discrepancies between SC and older experimental results may indicate errors in the experimental result.⁶⁵ However, more detailed analysis may be necessary to confirm this idea. Hence, it remains unknown which exactly are the correct rates in Fig. 11(b).

C. Nonequilibrium initial condition (constant-volume reactor)

The work presented so far all assume a thermochemical equilibrium condition before an instantaneous drop in translational

temperature which is then followed by nonequilibrium de-excitation occurring at a finite rate. However, in reality, it does not always have to be the case that a thermochemical equilibrium condition exists initially since the flow can get expanded before it achieves thermochemical equilibrium after the excitation event. Since the vibrational relaxation time scale is known to be smaller than the chemical reaction time scale,⁶⁷ there is a possibility of creating a pre-expansion condition with a high vibrational temperature but a low enough O mole fraction such that vibrational pumping occurs after the expansion.

To examine the possibility of this special scenario, excitation simulations are performed in constant-volume reactors at three different initial translational temperatures. The results are shown in Fig. 12(a) examining the vibrational excitation relative to the formation of O. When the initial translational temperature is 2200 K, one can see that the vibrational temperature reaches around 2000 K when the O mole

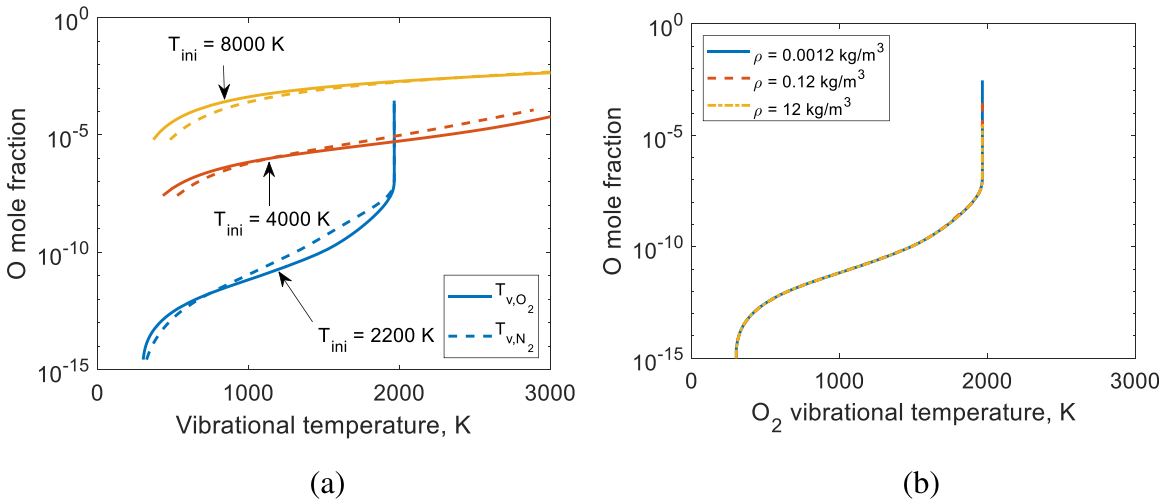


FIG. 12. The O mole fraction vs vibrational temperature profile during excitation in a constant-volume reactor at (a) three different initial translational temperatures (T_{ini}) and a density of 0.12 kg/m^3 , and (b) three different densities and $T_{ini} = 2200 \text{ K}$. The initial vibrational temperatures are 295 K in all cases.

03 November 2023 08:25:51

fraction is only around 10^{-8} . However, at the higher initial temperatures, the formation of O becomes significantly faster. Therefore, one may conclude that to generate the nonequilibrium state with the minimum amount of O at some vibrational temperature, the initial translational temperature has to be the minimum possible that can generate the vibrational temperature. For example, an initial translational temperature of 2200 K is just enough to generate a vibrational temperature of 2000 K with the O mole fraction being as low as 10^{-8} . Therefore, an O mole fraction of 10^{-8} is the minimum nonequilibrium value that can be attained at a vibrational temperature of 2000 K, which is much smaller than the equilibrium value of around 10^{-4} (at a density of 0.12 kg/m^3). Figure 12(a) also shows that, although large nonequilibrium between the vibrational and chemical modes is observed, the O_2 and N_2 vibrational modes are essentially equilibrated during the excitations in the temperature range shown, which is consistent with experimental observations in post-shock flows.⁴ Furthermore, Fig. 12(b) indicates that the O mole fraction vs O_2 vibrational temperature curve for excitation has essentially no pressure dependency. This is because the VVT and VT reactions are second-order reactions, and the chemical nonequilibrium during the vibrational excitation is dominated by the dissociation reaction (rather than the recombination reaction, which only becomes important as the relaxation approaches chemical equilibrium after thermal equilibration), which is also a second-order reaction. Therefore, all the relevant rates get scaled equally with pressure.

As shown in Fig. 3, an O mole fraction of 10^{-8} is low enough to prevent significant influence from the $\text{O}_2\text{-O}$ VT reaction and allow for vibrational pumping. Therefore, using the nonequilibrium condition at this time instance from the excitation simulation as the initial condition in a de-excitation simulation, the results are shown in Fig. 13. From Fig. 13(a), one can see that vibrational pumping is indeed observed. Also observed is further dissociation, despite the low translational temperature, which occurs during the first 10^{-2} s because the O

mole fraction is initially in nonequilibrium and too low relative to the O_2 vibrational temperature; this is a phenomenon earlier recognized in Ref. 4. The O mole fraction gets to more than 10^{-6} , which is enough to make the $\text{O}_2\text{-O}$ VT reaction significant, as shown in Fig. 13(b). The vibrational mode of O_2 gets pumped to a temperature of around 2100 K (pumping of $\approx 5\%$), which is about 200 K ($\approx 10\%$) lower than that which would have been seen if no further formation of O occurred (frozen chemistry) as shown in Fig. 13(a). Looking at the O_2 vibrational population distribution shown in Fig. 14(a), one can see that the distribution initially has an underpopulation in the upper levels which is typically seen in excitation conditions.⁴⁵ Pumping then causes the population in the intermediate and upper levels to increase as can be seen when comparing the results at 0, 1, and 10 ms. However, a Treanor distribution never forms due to the formation of significant amounts of O, which activates the $\text{O}_2\text{-O}$ VT reaction. Without additional production of O, a Treanor distribution would form, as shown in Fig. 14(b) for the frozen chemistry simulation, with population inversion in the intermediate and upper levels. As mentioned earlier, the $\text{O}_2\text{-O}$ VT reaction helps equilibrate the upper levels with the translational mode and prevents a population inversion in the upper levels. Eventually, by 20 ms, the ν_1 distribution is attained and the relaxation proceeds via this distribution.

The O_2 vibration-dissociation (VD) reactions $\text{O}_2(i) + \text{O}_2 \leftrightarrow 2\text{O} + \text{O}_2$ and $\text{O}_2(i) + \text{N}_2 \leftrightarrow 2\text{O} + \text{N}_2$ play an important role in the work presented in this subsection; these two VD reactions, with O_2 and N_2 being the collision partners, are the main routes to generate O in the conditions considered here. So, a discussion on the accuracy of the rates used for these reactions is necessary. The rate coefficients for these reactions, taken from the STELLAR database,⁴¹ were calculated using the FHO theory. These FHO rates were compared in Refs. 5, 36, and 68 against QCT and experimental results, and differences of up to around 1–2 orders of magnitude were observed, indicating some uncertainty here. More precisely, Refs. 5 and 68 showed that these

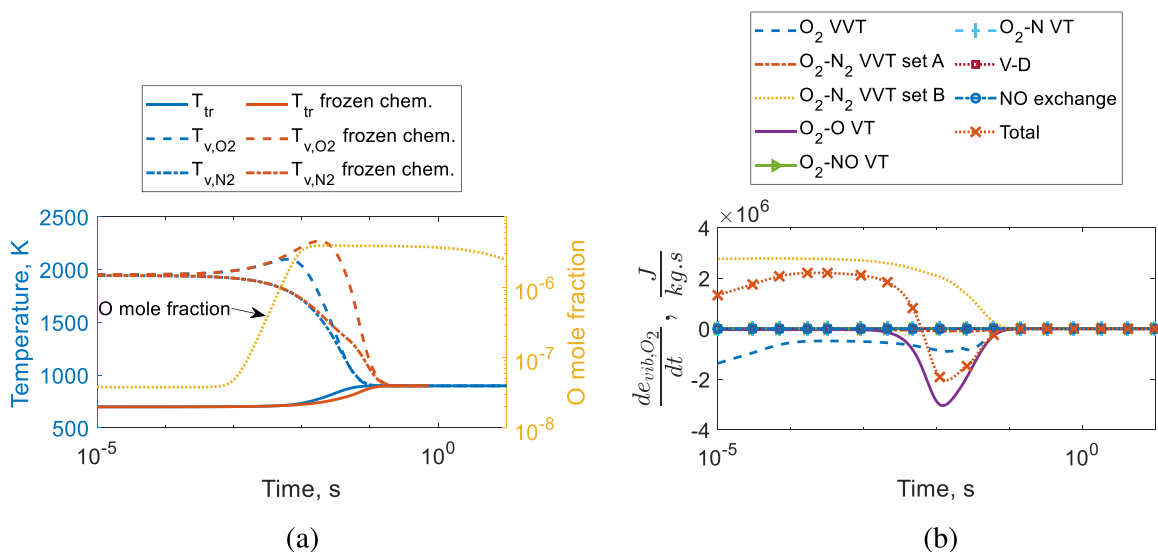


FIG. 13. The (a) temperature and mole fraction profile and (b) O_2 vibrational energy source terms for de-excitation from a nonequilibrium initial condition. This nonequilibrium initial condition is taken from the excitation simulation in Fig. 12 with $T_{ini} = 2200 \text{ K}$ and $\rho = 0.12 \text{ kg/m}^3$ at a point in time where $T_{v, \text{O}_2} = 1953.8 \text{ K}$ and O mole fraction is 3.8×10^{-8} .

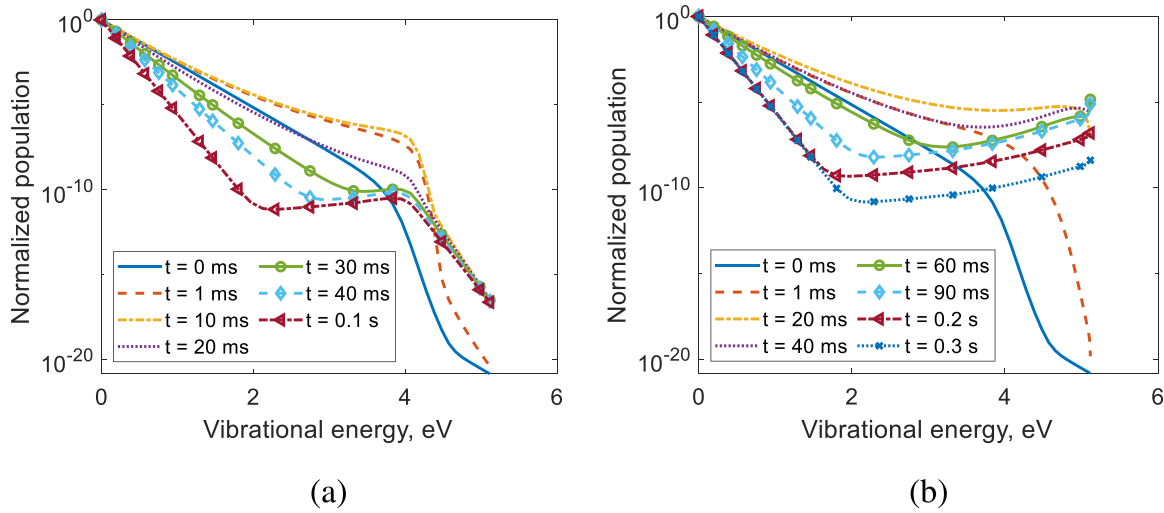


FIG. 14. Normalized O_2 vibrational population at various times in the (a) full and (b) frozen simulations in Fig. 13(a).

FHO dissociation rates were consistently lower than the experimental and QCT values. Then, if these FHO dissociation rates may be considered as being the lower bound, one may suggest that the degree of pumping shown in this subsection represents the upper bound because the lower dissociation rate lessens the formation of O, which allows for a larger degree of pumping.

So, the upper bound of pumping is only around 5% in both the equilibrium and nonequilibrium initial condition cases (presented in Secs. IV B and IV C, respectively). Because these initial conditions are selected based on Fig. 3 to lie within the region where the O_2-N_2 VVT set B (pumping) reaction is most dominant, and the uncertainty of the kinetic rates used in the simulations is shown to significantly favor pumping, one may consider the computed 5% to be a general upper bound for pumping. Consequently, it may be suggested that pumping is unimportant for practical intents and purposes, and there is no significant need to have multi-temperature models be able to qualitatively recreate this phenomenon. Although the pumping from O_2-N_2 VVT set B is still a significant contributor to the O_2 vibrational energy transfer throughout the relaxation in both cases, as shown in Figs. 8(b) and 13(b), and, consequently, influences the relaxation profile, this is not of significant concern as the numerous rates and parameters in the multi-temperature models can generally be tuned to adequately reproduce the same relaxation profile given the qualitative features can be captured first.^{69,70} Hence, while it would be impossible for multi-temperature models to capture the 5% pumping portion in the relaxation profile because the governing equations describe the vibrational relaxation as always moving toward equilibrium, appropriate parameter tuning should allow these models to quantitatively recreate the remainder of the relaxation profile to a sufficient extent.

D. Nozzle simulations

For completeness, it is now of interest to extend the constant-volume reactor results to actual gasdynamic situations. So, nozzle flows are examined in this subsection. The flow in nozzles usually

originates from a thermochemical equilibrium state at the throat.³³ Therefore, it is of interest to relate the situation in Sec. IV B, where the flow is initially in equilibrium (rather than the situation in Sec. IV C where the flow is initially in nonequilibrium) to nozzle flows. Quasi-one-dimensional nozzle simulations are performed for a 6° half-angle conical nozzle with a 30-mm-diameter throat, representative of hypersonic wind tunnel nozzles.³³ Larger angles do exist on the nozzle of propulsion devices because of the need to keep the nozzle length to a minimum, but the chemical composition of the flow in these nozzles is some combustion product and not air (the subject of the current work). As shown in Fig. 15, the simulation begins from the throat and then marches downstream in solving the ODE system given by Eq. (9), which solves an underexpanded nozzle (hypersonic wind tunnel nozzles always operate at underexpanded conditions). The throat is in equilibrium at a temperature of 1100 K—the initial equilibrium temperature from which pumping is shown to occur in Sec. IV B—and a velocity of 690 m/s giving a sonic condition. Three different throat pressures are tested— 10^6 , 10^7 , and 10^8 Pa—representative of practical hypersonic wind tunnel operating conditions.⁷¹

Space marching a distance of 0.23 m, the results are shown in Figs. 16(a), 16(c), and 16(e). In all cases, one can see that significant deviation forms between the vibrational modes and translational mode, with the deviation forming later with increasing throat pressure,

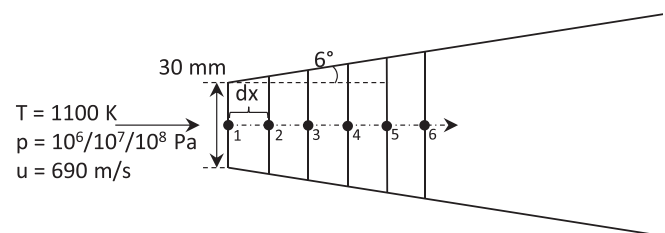


FIG. 15. Schematic diagram of the nozzle simulation.

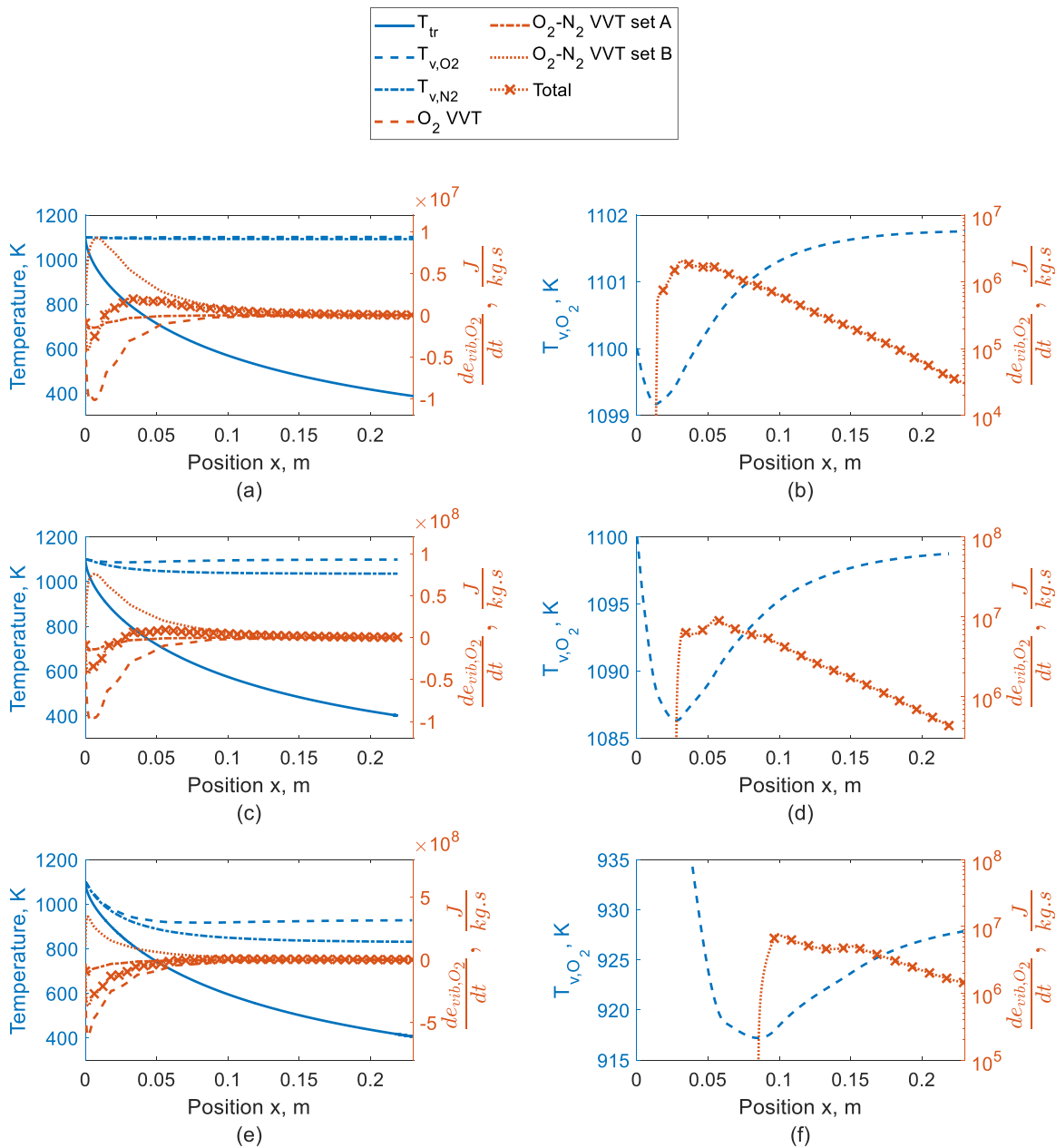


FIG. 16. The temperatures and O_2 vibrational energy source terms along a 6° half-angle conical nozzle with a 30-mm-diameter throat. The throat, at position $x = 0$ m, is in equilibrium at a temperature of 1100 K and pressure of (a) 10^6 Pa, (c) 10^7 Pa, and (e) 10^8 Pa. The zoomed-in view of the O_2 vibrational temperature and total O_2 vibrational energy source term is shown in (b), (d), and (f) for throat pressures of 10^6 , 10^7 , and 10^8 Pa, respectively.

as expected in nozzle flows.⁷² This same trend could also be achieved by varying the nozzle expansion angle, when considering the ratio of the characteristic fluidic and chemical time scales (Damköhler number), with the nonequilibrium forming later with decreasing angle. When a significant degree of nonequilibrium has formed between the translational mode and O_2 vibrational mode, the pumping contribution from O_2-N_2 set B overcomes the equilibrating contributions

(mainly from O_2-O_2 VVT) and the total source term becomes positive; this happens at around $x = 0.013$ m, $x = 0.028$ m, and $x = 0.085$ m in the 10^6 , 10^7 , and 10^8 Pa conditions, respectively. Pumping can then be observed as the O_2 vibrational temperature increases; this can be seen in the zoomed-in view shown in Figs. 16(b), 16(d), and 16(f). The rate of increase in the O_2 vibrational temperature (with respect to distance) decreases as the flow expands downstream and the source

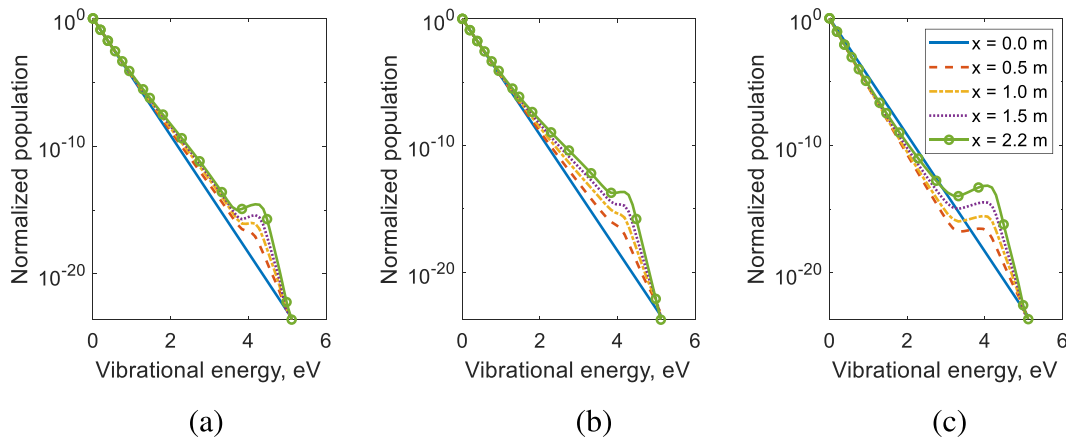


FIG. 17. Normalized O_2 vibrational population at various positions in the (a) 10^6 Pa, (b) 10^7 Pa, and (c) 10^8 Pa nozzle simulations shown in Fig. 16.

term gets smaller while the flow freezes. Signs of pumping are also observed in the population distribution, shown in Fig. 17, with energy flowing up the vibrational ladder causing an increased population of the intermediate and upper levels. As shown in Figs. 16(b), 16(d), and 16(f), pumping of around 3 K ($\approx 0.3\%$) can be observed in the 10^6 Pa condition, and pumping of around 10 K ($\approx 1\%$) can be observed in the 10^7 and 10^8 Pa conditions; all are less than the pumping of almost 50 K ($\approx 5\%$) seen in the equivalent constant-volume reactor in Sec. IV B.

It is of interest to relate the above nozzle results to relevant works (experimental and numerical) in the literature. To the best knowledge of the authors, measurement of the O_2 vibrational temperature in the air in a nozzle flow has never been done before. Even if such measurements exist, it would almost certainly be associated with an uncertainty that is too large (around $\pm 5\%$ – 20% as exemplified in Refs. 73 and 74) to allow for any convincing observation of pumping which, as shown in the current work, is small. Therefore, no experimental works are available for any meaningful comparison. More relevant numerical works can be found in Refs. 5 and 49, which contains quasi-one-dimensional StS nozzle simulations for air. No mention of vibrational pumping of O_2 was made in any of these works, which likely means this phenomenon did not manifest to any significant extent. This is therefore consistent with the current results.

As discussed in Ref. 48, important qualitative differences exist between a constant-volume reactor and some real (one-dimensional or multi-dimensional) gasdynamic scenario:

- (1) A constant-volume reactor assumes an infinitely fast expansion process that instantaneously produces a significantly nonequilibrium state before subsequent relaxation while, in reality, the expansion is generally more gradual.
- (2) No further expansion occurs during the relaxation process in a constant-volume reactor, whereas, for the particular case of nozzle flows, expansion occurs throughout, including after a significant degree of nonequilibrium is achieved.
- (3) Length scale is irrelevant in a constant-volume reactor, while length scale plays an important role in reality for determining the extent of the thermochemical relaxation that can be observed.

The above differences have nothing unique to do with the multi-dimensionality of flow and, thus, apply to both one-dimensional and multi-dimensional flows. Nevertheless, it is acknowledged that the multi-dimensionality of flow may, somehow, directly produce further distinctions from constant-volume reactors in terms of the thermochemical relaxation, but these would likely be subtler and more quantitative compared with the obvious qualitative differences listed above. In addition, the uncertainty of the kinetic rates used in the current simulations, examined in detail in Secs. IV B and C, is likely much more important than the simplification of the flowfield in terms of influencing the thermochemical relaxation process.

As discussed in Ref. 48, due to the differences listed above, zero-dimensional constant-volume reactors generally overestimate the manifestation of thermochemical nonequilibrium-associated phenomena when compared with equivalent one-dimensional and multi-dimensional flows. Thus, this along with the aforementioned fact that the kinetic rates used in the current simulations significantly favor pumping means the 5% upper bound for pumping, determined in Secs. IV B and C under zero-dimensional conditions, covers real gasdynamic scenarios. The second and third differences above are particularly important and are mainly why less pumping is observed in the nozzle compared with the equivalent constant-volume reactor. Consequently, as a corollary of these two differences, it can be suggested that constant-volume reactors are a better zero-dimensional analogy for the relaxation process in flows with large length scales and no further expansion after an initial rapid expansion. Examples of this include the flow along large distances downstream in the wake of an atmospheric entry vehicle, outside of the recirculating region, after the rapid expansion around the shoulder, and the flow along large distances in the acceleration tube of large-scale expansion tunnels⁷¹ (a type of hypersonic wind tunnel) after the rapid unsteady expansion originating from the secondary diaphragm rupture. The results in Sec. IV B can correspond to the common scenario in hypersonic flight where the flow achieves thermochemical equilibrium behind a shock before expansion over a convex corner. On the other hand, the results in Sec. IV C are more uncommon in flight as the relaxation process shown there may only occur on certain streamlines in the flow over a

hypersonic flight vehicle of a certain size flying at a certain attitude and velocity.

V. CONCLUSIONS

The occurrence of vibrational pumping in air under nonequilibrium conditions is investigated because this phenomenon is not considered in the formulation of the current phenomenological models. The competing processes in nonequilibrium air are examined to assess the possibility of self-pumping occurring for a general range of conditions. It is shown that O_2 , rather than N_2 , is the molecule that would get pumped due to its shallower vibrational well and smaller spacing between the vibrational levels. Pumping can only happen during de-excitation and when the translational temperature is below around 1000 K. Pumping will not occur when the initial equilibrium temperature is greater than around 1200–1600 K (depending on the pressure) due to the formation of enough O to quench pumping via the O_2 –O vibration–translation reaction. The limiting initial temperature can be increased to around 2000 K if a nonequilibrium initial condition is considered that has an O mole fraction significantly less than the equilibrium value. In cases where pumping does occur, constant–volume reactor simulations showed pumping of around 5%. Relaxation occurs via the Treanor distribution in the O_2 vibrational population when the O_2 –O VT reaction is irrelevant. The O_2 –O VT reaction promotes equilibration of the upper levels with the translational mode and, thus, relaxation occurs via the ν_1 distribution when the O_2 –O VT reaction is prominent. To consider real gasdynamic environments, quasi-one-dimensional nozzle simulations representative of hypersonic wind tunnel nozzle flows are conducted for pressures of 10^6 , 10^7 , and 10^8 Pa at the throat with an equilibrium temperature of 1100 K. Pumping of around 3 K ($\approx 0.3\%$) can be observed in the 10^6 Pa condition, and pumping of around 10 K ($\approx 1\%$) can be observed in the 10^7 and 10^8 Pa conditions. Freezing, which is expected given the short length scale of nozzles and the fact that nozzle flows continue to expand after pumping starts, limits the degree of pumping seen in the nozzle flows. It can be suggested that constant–volume reactors generally overestimate the manifestation of thermochemical nonequilibrium-associated phenomena, when compared with practical flow scenarios, and are a better zero-dimensional analogy for the relaxation process in flows with large length scales and no further expansion after an initial rapid expansion, such as in the wake of atmospheric entry vehicles and the acceleration tube of large-scale expansion tunnels. After examination of the uncertainties of the most important rates used in the simulations, which are the $O_2(1) + N_2(0) \leftrightarrow O_2(0) + N_2(1)$ VV and $O_2(1) + O_2(0) \leftrightarrow O_2(0) + O_2(0)$ VT rates as well as the $O_2(i) + O_2 \leftrightarrow 2O + O_2$ and $O_2(i) + N_2 \leftrightarrow 2O + N_2$ VD rates when a nonequilibrium initial condition is considered, one may suggest that the current results correspond to the upper bound for the magnitude of pumping. It may be concluded that pumping is unimportant for practical intents and purposes in nonequilibrium hypersonic flows, and there is no significant need to have phenomenological models be able to recreate this phenomenon. Nevertheless, knowledge of this would have been impossible without the work presented in this paper.

ACKNOWLEDGMENTS

This work was supported by the National Natural Science Foundation of China (No. 12202373).

AUTHOR DECLARATIONS

Conflict of Interest

The authors have no conflicts to disclose.

Author Contributions

Sangdi Gu: Conceptualization (lead); Data curation (lead); Formal analysis (lead); Funding acquisition (lead); Investigation (lead); Methodology (lead); Software (lead); Writing – original draft (lead); Writing – review & editing (equal). **Jiaao Hao:** Formal analysis (supporting); Supervision (equal); Writing – review & editing (equal). **Chih-Yung Wen:** Formal analysis (supporting); Supervision (equal); Writing – review & editing (equal).

DATA AVAILABILITY

The data that support the findings of this study are available within the article.

REFERENCES

- J. W. Rich, S. O. Macheret, and I. V. Adamovich, “Aerothermodynamics of vibrationally nonequilibrium gases,” *Exp. Therm. Fluid Sci.* **13**(1), pp. 1–10 (1996).
- C. Park and S.-H. Lee, “Validation of multitemperature nozzle flow code,” *J. Thermophys. Heat Transfer* **9**(1), 9–16 (1995).
- M. J. Wright, F. S. Milos, and P. Tran, “Afterbody aeroheating flight data for planetary probe thermal protection system design,” *J. Spacecr. Rockets* **43**(5), 929–943 (2006).
- C. Park, *Nonequilibrium Hypersonic Aerothermodynamics* (Wiley, New York, 1989), p. 358.
- C. Park, “Thermochemical relaxation in shock tunnels,” *J. Thermophys. Heat Transfer* **20**(4), 689–698 (2006).
- S. Gu, J. Hao, Q. Wang, and C.-Y. Wen, “Influence of thermochemical nonequilibrium on expansion tube air test conditions: A numerical study,” *Phys. Fluids* **35**(3), 036106 (2023).
- I. Nompelis, G. V. Candler, and M. S. Holden, “Effect of vibrational nonequilibrium on hypersonic double-cone experiments,” *AIAA J.* **41**(11), 2162–2169 (2003).
- F. Liu and L. Bao, “Peak heat flux prediction of hypersonic flow over compression ramp under vibrationally excited free-stream condition,” *Phys. Fluids* **35**(1), 016120 (2023).
- J. Hao and C.-Y. Wen, “Effects of vibrational nonequilibrium on hypersonic shock-wave/laminar boundary-layer interactions,” *Int. Commun. Heat Mass Transfer* **97**, 136–142 (2018).
- A. D. Cutler *et al.*, “Nonequilibrium supersonic freestream studied using coherent anti-Stokes Raman spectroscopy,” *AIAA J.* **53**(9), 2762–2770 (2015).
- R. Miles, A. Dogariu, and L. Dogariu, “Localized time accurate sampling of non-equilibrium and unsteady hypersonic flows: Methods and horizons,” *Exp. Fluids* **62**(12), 248 (2021).
- J. W. Rich, “Kinetic modeling of the high-power carbon monoxide laser,” *J. Appl. Phys.* **42**(7), 2719–2730 (1971).
- C. Park, “Review of chemical-kinetic problems of future NASA missions. I. Earth entries,” *J. Thermophys. Heat Transfer* **7**(3), 385–398 (1993).
- C. E. Treanor, J. Rich, and R. Rehm, “Vibrational relaxation of anharmonic oscillators with exchange-dominated collisions,” *J. Chem. Phys.* **48**(4), 1798–1807 (1968).
- S. Gu, J. Hao, and C.-Y. Wen, “State-specific study of air in the expansion tunnel nozzle and test section,” *AIAA J.* **60**(7), 4024–4038 (2022).
- A. Munafo, A. Lani, A. Bultel, and M. Panesi, “Modeling of non-equilibrium phenomena in expanding flows by means of a collisional-radiative model,” *Phys. Plasmas* **20**(7), 073501 (2013).
- M. Nishida and M. Matsumoto, “Thermochemical nonequilibrium in rapidly expanding flows of high-temperature air,” *Z. Naturforsch. A* **52**(4), 358–368 (1997).

- ¹⁸G. V. Candler and R. W. McCormack, "Computation of weakly ionized hypersonic flows in thermochemical nonequilibrium," *J. Thermophys. Heat Transfer* **5**(3), 266–273 (1991).
- ¹⁹K. E. Shuler, "Relaxation of an isolated ensemble of harmonic oscillators," *J. Chem. Phys.* **32**(6), 1692–1697 (1960).
- ²⁰J. D. Anderson, *Gasdynamic Lasers: An Introduction* (Academic Press, London, 1976).
- ²¹J. D. Anderson, Jr., "Gasdynamic lasers: Review and extension," *Acta Astronaut.* **2**(11–12), 911–927 (1975).
- ²²S. A. Losev, *Gasdynamic Laser*, 1st ed., Springer Series in Chemical Physics (Springer, Berlin, Heidelberg, 1981).
- ²³J. W. Rich and C. E. Treanor, "Vibrational relaxation in gas-dynamic flows," *Annu. Rev. Fluid Mech.* **2**(1), 355–396 (1970).
- ²⁴R. L. McKenzie, "Diatom gasdynamic lasers," *Phys. Fluids* **15**(12), 2163–2173 (1972).
- ²⁵E. T. Gerry, "Gasdynamic lasers," *IEEE Spectr.* **7**(11), 51–58 (1970).
- ²⁶R. Greenberg, A. Schneiderman, D. Ahouse, and E. Parmentier, "Rapid expansion nozzles for gas dynamic lasers," *AIAA J.* **10**(11), 1494–1498 (1972).
- ²⁷S. Losev and V. Makarov, "Optimization of the gain of a carbon dioxide gasdynamic laser," *Sov. J. Quantum Electron.* **4**(7), 905–909 (1975).
- ²⁸S. A. Losev and V. Makarov, "Multifactor optimization of a carbon dioxide gasdynamic laser. I. Gain optimization," *Sov. J. Quantum Electron.* **5**(7), 780–783 (1975).
- ²⁹S. Lam, "An analytical theory of vibrational relaxation for anharmonic molecules under strongly pumped conditions," *J. Chem. Phys.* **67**(6), 2577–2584 (1977).
- ³⁰J. D. Anderson, "High-Temperature flows," in *Modern Compressible Flow: With Historical Perspective*, 4th ed. (McGraw-Hill, New York, 2021), Chap. 17.
- ³¹J. D. Anderson, *Hypersonic and High-Temperature Gas Dynamics*, AIAA Education Series (American Institute of Aeronautics and Astronautics, Reston, VA, 2019).
- ³²H. Bailey, "Numerical integration of the equations governing the one-dimensional flow of a chemically reactive gas," *Phys. Fluids* **12**(11), 2292–2300 (1969).
- ³³S. Gu, J. Hao, and C.-Y. Wen, "Air thermochemistry in the converging section of de Laval nozzles on hypersonic wind tunnels," *AIP Adv.* **12**(8), 085320 (2022).
- ³⁴C. F. Curtiss and J. O. Hirschfelder, "Integration of stiff equations," *Proc. Natl. Acad. Sci.* **38**(3), 235–243 (1952).
- ³⁵S. Gu, J. Hao, and C.-Y. Wen, "On the vibrational state-specific modelling of radiating normal-shocks in air," *AIAA J.* **60**(6), 3760–3774 (2022).
- ³⁶M. Lino da Silva, J. Loureiro, and V. Guerra, "A multiquantum dataset for vibrational excitation and dissociation in high-temperature O₂-O₂ collisions," *Chem. Phys. Lett.* **531**, 28–33 (2012).
- ³⁷M. Lino da Silva, V. Guerra, and J. Loureiro, "State-resolved dissociation rates for extremely nonequilibrium atmospheric entries," *J. Thermophys. Heat Transfer* **21**(1), 40–49 (2007).
- ³⁸I. V. Adamovich, S. O. Macheret, J. W. Rich, and C. E. Treanor, "Vibrational energy transfer rates using a forced harmonic oscillator model," *J. Thermophys. Heat Transfer* **12**(1), 57–65 (1998).
- ³⁹F. Esposito and M. Capitelli, "The relaxation of vibrationally excited O₂ molecules by atomic oxygen," *Chem. Phys. Lett.* **443**(4–6), 222–226 (2007).
- ⁴⁰W. Su, D. Bruno, and Y. Babou, "State-specific modeling of vibrational relaxation and nitric oxide formation in shock-heated air," *J. Thermophys. Heat Transfer* **32**(2), 337–352 (2018).
- ⁴¹M. Lino da Silva, B. Lopez, V. Guerra, and J. Loureiro, "A multiquantum state-to-state model for the fundamental states of air: The stellar database," in *Proceedings of 5th International Workshop on Radiation of High Temperature Gases in Atmospheric Entry*, Barcelona, Spain, 16–19 October (ESASP, Noordwijk, The Netherlands, 2012), Vol. 714, p. 16.
- ⁴²F. Esposito, I. Armenise, and M. Capitelli, "N–N₂ state to state vibrational-relaxation and dissociation rates based on quasiclassical calculations," *Chem. Phys.* **331**(1), 1–8 (2006).
- ⁴³D. Bose and G. V. Candler, "Thermal rate constants of the N₂ + O → NO + N reaction using ab initio 3A⁺ and 3A⁺ potential energy surfaces," *J. Chem. Phys.* **104**(8), 2825–2833 (1996).
- ⁴⁴D. Bose and G. V. Candler, "Thermal rate constants of the O₂ + N → NO + O reaction based on the A² and A⁴ potential-energy surfaces," *J. Chem. Phys.* **107**(16), 6136–6145 (1997).
- ⁴⁵J. Hao, J. Wang, and C. Lee, "State-specific simulation of oxygen vibrational excitation and dissociation behind a normal shock," *Chem. Phys. Lett.* **681**, 69–74 (2017).
- ⁴⁶M. S. Grover, P. Valentini, E. Josyula, and R. S. Chaudhry, "Vibrational state-to-state and multiquantum effects for N₂ + N₂ interactions at high temperatures for aerothermodynamic applications," AIAA Paper No. 2020-1227, 2020.
- ⁴⁷B. Lopez and M. Lino Da Silva, "Non-Boltzmann analysis of hypersonic air re-entry flows," AIAA Paper No. 2014-2547, 2014.
- ⁴⁸S. M. Ruffin, "Prediction of vibrational relaxation in hypersonic expanding flows. II. Results," *J. Thermophys. Heat Transfer* **9**(3), 438–445 (1995).
- ⁴⁹S. F. Gimelshein and I. J. Wysong, "Nonequilibrium effects in high enthalpy gas flows expanding through nozzles," *Phys. Fluids* **33**(10), 106104 (2021).
- ⁵⁰G. Oblapenko, "Calculation of vibrational relaxation times using a kinetic theory approach," *J. Phys. Chem. A* **122**(50), 9615–9625 (2018).
- ⁵¹D. A. Andrienko and I. D. Boyd, "Master equation study of vibrational and rotational relaxations of oxygen," *J. Thermophys. Heat Transfer* **30**(3), 533–552 (2016).
- ⁵²J. Breen, R. Quay, and G. Glass, "Vibrational relaxation of O₂ in the presence of atomic oxygen," *J. Chem. Phys.* **59**(1), 556–557 (1973).
- ⁵³J. H. Kiefer and R. W. Lutz, "The effect of oxygen atoms on the vibrational relaxation of oxygen," *Symp. (Int.) Combust.* **11**(1), 67–76 (1967).
- ⁵⁴L. Ibragimova, A. Sergievskaya, V. Y. Levashov, O. Shatalov, Y. V. Tunik, and I. Zabelinskii, "Investigation of oxygen dissociation and vibrational relaxation at temperatures 4000–10800 K," *J. Chem. Phys.* **139**(3), 034317 (2013).
- ⁵⁵See <https://www.cantera.org> for "Cantera: An object-oriented software toolkit for chemical kinetics, thermodynamics, and transport processes," 2021.
- ⁵⁶A. Guy, A. Bourdon, and M.-Y. Perrin, "Consistent multi-internal-temperatures models for nonequilibrium nozzle flows," *Chem. Phys.* **420**, 15–24 (2013).
- ⁵⁷C. Hsu and L. D. McMillen, "Time-dependent solutions for de-excitation rates of anharmonic oscillators," *J. Chem. Phys.* **56**(11), 5327–5334 (1972).
- ⁵⁸K. N. Bray, "Vibrational relaxation of anharmonic oscillator molecules: Relaxation under isothermal conditions," *J. Phys. B: At. Mol. Phys.* **1**(4), 705 (1968).
- ⁵⁹G. Caledonia and R. Center, "Vibrational distribution functions in anharmonic oscillators," *J. Chem. Phys.* **55**(2), 552–561 (1971).
- ⁶⁰G. D. Billing and R. Kolesnick, "Vibrational relaxation of oxygen. State to state rate constants," *Chem. Phys. Lett.* **200**(4), 382–386 (1992).
- ⁶¹C. Coletti and G. D. Billing, "Vibrational energy transfer in molecular oxygen collisions," *Chem. Phys. Lett.* **356**(1–2), 14–22 (2002).
- ⁶²Q. Hong *et al.*, "Energy exchange rate coefficients from vibrational inelastic O₂ (³Σ_g⁻) + O₂ (³Σ_g⁻) collisions on a new spin-averaged potential energy surface," *J. Chem. Phys.* **154**(6), 064304 (2021).
- ⁶³S. Ormonde, "Vibrational relaxation theories and measurements," *Rev. Mod. Phys.* **47**(1), 193–258 (1975).
- ⁶⁴D. A. Andrienko and I. D. Boyd, "Kinetic models of oxygen thermochemistry based on quasi-classical trajectory analysis," *J. Thermophys. Heat Transfer* **32**(4), 904–916 (2018).
- ⁶⁵E. Garcia, A. Kurnosov, A. Laganà, F. Pirani, M. Bartolomei, and M. Cacciatore, "Efficiency of collisional O₂ + N₂ vibrational energy exchange," *J. Phys. Chem. B* **120**(8), 1476–1485 (2016).
- ⁶⁶R. L. Taylor and S. Bitterman, "Survey of vibrational relaxation data for processes important in the CO₂-N₂ laser system," *Rev. Mod. Phys.* **41**(1), 26–47 (1969).
- ⁶⁷P. Kim, "Non-equilibrium effects on hypersonic turbulent boundary layers," Ph.D. thesis (Mechanical and Aerospace Engineering Department, University of California, Los Angeles, 2016).
- ⁶⁸D. A. Andrienko and I. D. Boyd, "State-specific dissociation in O₂-O₂ collisions by quasiclassical trajectory method," *Chem. Phys.* **491**, 74–81 (2017).
- ⁶⁹B. A. Cruden and A. M. Brandis, "Measurement and prediction of radiative nonequilibrium for air shocks between 7–9 km/s," AIAA Paper No. 2017-4535, 2017.
- ⁷⁰H. H. Reising, T. W. Haller, N. T. Clemens, P. L. Varghese, R. Fiévet, and V. Raman, "Spontaneous Raman scattering temperature measurements and large eddy simulations of vibrational non-equilibrium in high-speed jet flames," AIAA Paper No. 2016-3550.

⁷¹S. Gu and H. Olivier, "Capabilities and limitations of existing hypersonic facilities," *Prog. Aerosp. Sci.* **113**, 100607 (2020).

⁷²J. G. Hall and C. E. Treanor, see <https://www.sto.nato.int/publications/AGARD/AGARD-AG-124/AGARD-AG-124.pdf> for "Nonequilibrium effects in supersonic-nozzle flows, 1967," AGARDograph No. 124.

⁷³J. Girard *et al.*, "Measurements of reflected shock tunnel freestream nitric oxide temperatures and partial pressure," *AIAA J.* **59**(12), 5266–5275 (2021).

⁷⁴P. M. Finch *et al.*, "Measurements of T5 shock tunnel freestream temperature, velocity, and composition," *AIAA J.* **61**(4), 1555–1578 (2023).